Spectral analysis of χ class data of GRS 1915+105 using TCAF solution

RAA 2020 Vol. **20** No. **12**, 208(10pp) doi: 10.1088/1674-4527/20/12/208

http://www.raa-journal.org *http://iopscience.iop.org/raa*

***R**esearch in*
***A**stronomy and*
***A**strophysics*

Spectral analysis of χ class data of GRS 1915+105 using TCAF solution

Anuvab Banerjee[1], Ayan Bhattacharjee[1], Dipak Debnath[2⋆] and Sandip K. Chakrabarti[2]

[1] S. N. Bose National Centre for Basic Sciences, Block-JD, Sector-3, Salt Lake, Kolkata, 700106, India
[2] Indian Centre for Space Physics, 43 Chalantika, Garia St. Rd., Kolkata, 700084, India; *anuvab.banerjee@bose.res.in, ayan12@bose.res.in, dipakcsp@gmail.com, sandip@csp.res.in*

Received 2020 February 20; accepted 2020 June 4

Abstract The class variable source GRS 1915+105 exhibits a wide range of time variabilities on timescales of a few seconds to a few days. Depending on the count rates in different energy bands and the nature of the conventional color-color diagram, the variabilities were classified into sixteen classes that were later sequenced in ascending order of Comptonization Efficiency (CE), which is the ratio of power-law and blackbody photons. However, CE estimation is based on an empirical model which does not provide us with a comprehensive picture regarding accretion flow dynamics around the central source. In reality, the accretion flow is comprised of two components: the high angular momentum Keplerian flow in the form of a radiatively efficient disk and a low angular momentum radiatively inefficient sub-Keplerian halo enveloping the disk. These two components contribute differently to the overall flux due to the differences in their radiative efficiencies. Therefore, it is necessary to analyze the spectral behaviors and time variabilities in terms of accretion rates. In χ class, X-ray flux is steady with no significant variation, however various χ subclasses are observed at different X-ray fluxes and variations of count rates across different χ subclasses must be linked to the variation of flow parameters such as the accretion rates, be it the Keplerian disk rate and/or the low angular momentum halo rate. This motivated us to analyze the spectra of the χ class data implementing the physical Two Component Advective Flow (TCAF) solution which directly extracts these two rates from spectral fits. We find that in the $\chi_{2,4}$ classes, which are reportedly devoid of significant outflows, the spectra could be fitted well applying the TCAF solution alone. In the $\chi_{1,3}$ classes, which are always linked with outflows, a cutoff power-law model is needed in addition to the TCAF solution. At the same time, the normalization required by this model along with the variation of photon index and exponential roll-off factor provides us with information on the relative dominance of the outflow in the latter two classes. TCAF fit also supplies us with the size and location of the Compton cloud along with its optical depth. Thus by fitting with TCAF, a physical understanding of the flow geometry in different χ classes of GRS 1915+105 has been obtained.

Key words: X-Rays: binaries — stars: individual (GRS 1915+105) — stars: black holes — accretion, accretion disks — ISM: jets and outflows — radiation: dynamics

1 INTRODUCTION

It has been noted right since the discovery of the Galactic black hole (BH) X-ray binary (BHXB) GRS 1915+105 that it exhibits persistent brightness (Remillard & McClintock 2006). A complex timing and spectral variability pattern over a wide span of timescales from a few seconds to a few days as revealed through continuous X-ray monitoring is also an important characteristic of this source (Greiner et al. 1996; Morgan et al. 1997; Klein-Wolt et al. 2002). This variability pattern was grouped into several classes on the basis of the ratio of photon count rates in different energy bands (hardness ratio) and the color-color diagrams obtained from these ratios (Yadav et al. 1999; Muno et al. 1999; Belloni et al. 2000). The χ classes are devoid of strong temporal and spectral variabilities. The subclasses $\chi_{1,3}$ are associated with strong radio jets (Naik & Rao 2000; Vadawale et al. 2001, 2003) while the subclasses $\chi_{2,4}$ do not show such behavior.

Since the nature of the hardness ratio or color-color diagram depends on the choice of energy bands for the soft and hard photons, and therefore, on the mass of the BH, an alternate mass independent description of these

⋆ Corresponding author

variability classes was published (Pal et al. 2013) in terms of the Comptonization Efficiency (CE) which, in reality, is a dynamic hardness ratio, given by the instantaneous ratio of the number of photons under the power-law (N_p) and the number of photons under multi-color blackbody (N_b) component of the composite spectra. When CE (=N_p/N_b) is arranged in ascending order, the classes appear to be arranged in the same order. Since N_p is nothing but a fraction of N_b which is intercepted by the Compton cloud, CE also gives an idea of the flow configuration - a large CE would mean a large Compton cloud, which will necessarily yield a hard state. In this sequence, χ naturally appears at the end, where the spectra are the hardest. In this scheme, similar 'looking' classes as far as the light curves go, have similar CEs and the sequence is also the same for other objects (e.g., IGR 17091–3624) which exhibit variability classes (Pal & Chakrabarti 2015).

Successful spectral fits and extraction of accretion flow parameters were achieved for a large number of transient BH sources (Debnath et al. 2014, 2015b,a, 2017; Debnath 2018; Debnath et al. 2020; Mondal et al. 2014, 2016; Chatterjee et al. 2016, 2019; Jana et al. 2016, 2017, 2020a,b; Molla et al. 2016; Bhattacharjee et al. 2017; Shang et al. 2019; Chatterjee et al. 2020) with a two component flow solution which is a natural outcome of a viscous transonic flow (Chakrabarti 1995, 1997 and references therein). Recently, the same paradigm has also been applied in the case of persistent sources and weakly magnetized neutron stars with requisite modifications (Banerjee et al. 2019; Bhattacharjee & Chakrabarti 2017, 2019; Bhattacharjee 2018). This so-called Two Component Advective Flow (TCAF) solution envisages that due to a vertical gradient of viscous processes, the injected low angular momentum matter would disaggregate into an equatorial plane based Keplerian disk emitting soft X-rays surrounded by a low angular momentum halo forming a centrifugal barrier close to the BH and emitting Comptonized hard X-rays. The centrifugal barrier could be so strong that the flow piles up against it forming a standing shock and the subsonic post-shock region is the CENtrifugal pressure supported BOundary Layer or CENBOL. This acts like a boundary layer and is also responsible for supplying matter to form outflows (Chakrabarti 1999). Beyond the shock location, the Keplerian and sub-Keplerian components are mixed and, therefore, the shock location acts as the truncation radius in the TCAF paradigm. Giri & Chakrabarti (2013) established, through numerical simulations, that the TCAF solution is a stable configuration. In the harder states, the CENBOL cannot be cooled by inverse Comptonization (e.g., Sunyaev & Titarchuk 1980, 1985) due to low disk accretion rate and thus outflow is produced. In soft states, the CENBOL is completely cooled down and collapses due to high Keplerian disk rate and no outflow can form. This is also established by detailed hydrodynamic simulations with Compton processes (Garain et al. 2012). It has been demonstrated also that the ratio of the outflow rate to inflow rate is highest if the shock compression ratio is moderate (Chakrabarti 1999) and this outflow takes part in Comptonization and plays a major role in deciding the nature of the light curves of GRS 1915+105 (Chakrabarti & Manickam 2000).

In the literature, X-ray spectral properties of GRS 1915+105 have been studied by several authors over the years (Fender & Belloni 2004; Remillard & McClintock 2006; McClintock & Remillard 2006; Pal et al. 2013; Pal & Chakrabarti 2015; Peris et al. 2016). It has also been a key source in understanding the disk-jet connection in the context of X-ray binaries (Vadawale et al. 2003; Fender et al. 2004). The radio flares have been subdivided into two categories on the basis of the properties of accretion disk evolution: (1) Persistent radio flare where the accretion disk remains steady. In this case, inflow and outflow are in equilibrium and there is no sudden change in either the soft or hard component. (2) Other flares which are associated with changes in the accretion disk. Here the hard and soft components are affected and the object proceeds towards a state transition (Yadav 2001, 2006). Pal et al. (2013); Pal & Chakrabarti (2015) studied such phenomena mainly with the spectral fits applying phenomenological power-law and disk blackbody models and they also obtained the hardness of the object in different timing classes. However, to the best of our knowledge, no work has been undertaken which computes the accretion rates and properties of the Compton cloud for any of the variable classes. Just like the TCAF model is employed to study the accretion flow dynamics of the outbursting sources (Debnath et al. 2014, 2015b), the same fitting procedure could be followed for GRS 1915+105 as well to study the dependence of class behaviors on flow parameters.

In the present paper, we concentrate on the analysis of χ class data from the Rossi X-ray Timing Explorer (RXTE) satellite to determine the flow parameters. In the next section, we first give a theoretical background on the flow configuration as expected from the TCAF solution and how winds might be formed which affect the spectra in this class of solutions. In Section 3, we analyze the data. In Section 4, we present our results. Finally, in Section 5, we give the concluding remarks.

2 THEORETICAL BACKGROUND

It is normally assumed that a Keplerian flow is supplied at the outer edge of a BH accretion disk by the companion. However, observations of several binary systems clearly suggest that two components are necessary to explain

the timing properties as proposed by Chakrabarti in 1997 (Chakrabarti 1997; Smith et al. 2002; Wu et al. 2002; Ghosh & Chakrabarti 2019). Subsequently, it was shown that the jets and outflows are launched at the CENBOL and the outflow rate depends on the compression ratio of the shock which is responsible for forming the CENBOL (Chakrabarti 1999, hereafter C99). The nature of the two component inflow configurations across the spectral states and when the outflows are expected to be highest have been discussed in Chakrabarti et al. (2000); Chakrabarti & Nandi (2000).

In Figure 1(a,b), adopted from Chakrabarti et al. (2000), we illustrate the two possible flow configurations leading to $\chi_{2,4}$ and $\chi_{1,3}$ temporal states respectively. In Figure 1(a), we display the standard flow configuration around the BH consisting of both Keplerian and sub-Keplerian matter. If the shock conditions are satisfied and the viscosity is so small that the Keplerian disk rate is still low, the outflow may launch from close to the BH until the optical depth of the sonic sphere at the base of the outflow is low. Satisfaction of these conditions also allows the outflow to be a steady. This configuration is depicted in Figure 1(b) (also see C99). Initially, as the shock strength rises from unity, the outflow rate would also rise (C99). When the optical depth of the sonic sphere crosses unity, the outflow will separate out as a blobby jet component and the cooler matter returns back to the inflow (Chakrabarti & Nandi 2000). This creates the so-called 'burst-on' state. When the return flow is drained out, a 'burst-off' state is created. A further rise in the shock strength would reduce the outflows in comparison to inflows. When the viscosity is high enough to enhance the Keplerian disk rate, it cools the CENBOL, quenches the outflow and a soft state is created.

In recent times as the TCAF paradigm has been well studied in the case of outbursting sources, we ventured to extend our spectral studies to the class variable source GRS 1915+105 as well to obtain a possible picture of accretion flow dynamics around such objects. Muno et al. (1999) and McClintock & Remillard (2006) reported that classes with steady fluxes from GRS 1915+105 often resemble hard states of persistent sources. In the spectral and temporal study of this object by Rao et al. (2000), to pin down the source of the hard photons to be the CENBOL, the spectra of χ_3 class were also fitted using combined disk blackbody (diskbb), CompST and cutoff power-law (diskbb+CompST+cutoffpower-law). Since for χ classes the fluxes are almost steady, we were motivated to do the spectral analysis applying the TCAF model on χ classes. Since in TCAF, the contributions from disk and Comptonization from the CENBOL are self-consistently accounted for by solving a radiative transfer equation, there is no requirement for separate models

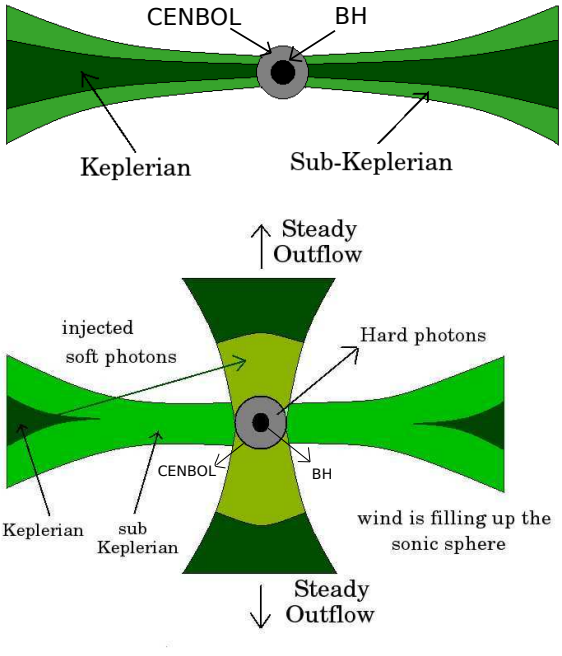

Fig. 1 (a) The accretion flow consisting of Keplerian and sub-Keplerian flow. Their relative abundance dictates the hardness and softness of the state. This configuration corresponds to the $\chi_{2,4}$ classes. (b) A shock is produced due to satisfaction of Rankine-Hugoniot conditions. In both of the figures, the grey shaded region around the BH represents the CENBOL. Outflow is generated and a steady outflow rate is maintained because the average optical depth within the sonic sphere is smaller than unity. This corresponds to the $\chi_{1,3}$ classes (adopted from Chakrabarti et al. 2000).

like diskbb and CompST. However, to account for the additional Comptonization from the outflow, other models like cutoff power-law (cutoffpl) might be required.

According to the reports in literature, mass of the source is believed to be well established. It was first estimated to be $14 \pm 4\ M_\odot$ (Greiner et al. 2001). Investigating the optical counterpart, the mass of the donor was found to be $\sim 1.2\ M_\odot$, implying the source to be a low-mass X-ray binary. A further estimate of $12.4^{+2.0}_{-1.8}\ M_\odot$ was found by trigonometric parallax measurement (Reid et al. 2014). However, mass is the intrinsic property of the BH and not a flow parameter. Therefore, for the purpose of our analysis, we have kept the mass of the BH frozen at $14\ M_\odot$, while fitting spectra with the TCAF model fits file.

3 DATA SELECTION AND THE METHOD OF ANALYSIS

For the spectral analysis, RXTE science data from NASA HEASARC data archive are utilized. We consider one each of $\chi_1, \chi_2, \chi_3, \chi_4$ class data as reported in Pal et al. (2013) and continuous observation span is divided into

several slices to carry out spectral analysis over each one of the segments separately in order to have better statistics on fitted parameters. HEASARC's spectra generating software package HEASOFT version HEADAS 6.18 and XSPEC version 12.8.2 have been used for the extraction and analysis of the spectra. For the generation of '.pha' files and fitting of the spectra using the TCAF solution, the procedure described by Debnath et al. (2013, 2014) has been employed. The *standard2* mode Science Data of the PCA instrument was utilized for spectral analysis. For each observational ID, the spectrum was extracted from all the Xenon layers of PCU2 containing 128 channels, without any grouping. The PCA background was extracted by the 'runpcabackest' command and then the latest bright-source background model was applied. In order to take care of the South Atlantic Anomaly (SAA), the PCA SAA History file was incorporated and the data acquired during the SAA passage and for elevation less than 10° and offset less than 0.02 were excluded. The $2.5 - 25$ keV background subtracted spectra were fitted by a TCAF based additive model fits file. We have checked that the spectral fitting up to higher energy does not change the qualitative conclusions that we have made, hence we have confined ourselves to be in the aforementioned energy domain. The 'err' command was executed to determine the 90% confidence error values of the model fitted parameters.

In order to take care of the interstellar absorption, the multiplicative model *phabs* was employed. While in Muno et al. (1999), the hydrogen column density was kept fixed at 6.0×10^{22} atoms cm^{-2}, it was kept frozen at 5.0×10^{22} atoms cm^{-2} in the process of fitting the steady state spectra by other observers (Lee et al. 2002; Peris et al. 2016). The column density was also maintained in the range $(4.5 - 7.0) \times 10^{22}$ atoms cm^{-2} by Peris et al. (2016), but no significant departure of the fitted parameters was noticed. While analyzing the low/hard state of GRS 1915+105 to measure the spin, Blum et al. (2009) regarded the absorption column density to be 4.0×10^{22}. On the other hand, while measuring the correlation between disk parameters and superluminal jet parameters, N_H had been considered to be at a higher value of $(10.0 - 15.0) \times 10^{22}$ (Yadav 2006). Throughout our analysis, we found N_H to be in the range $(4.5 - 7.5) \times 10^{22}$.

The PCA data IDs chosen for the analysis of χ_2 and χ_4 class data respectively are 20402–01–16–00 (MJD=50501) and 10408–01–33–00 (MJD=50333). For χ_1 and χ_3 classes, we utilized PCA data of observation IDs 10408–01–23–00 (MJD=50278) and 20402–01–50–00 (MJD=50735) respectively. The $\chi_{2,4}$ class data are fitted with only the TCAF solution based model *fits* file, for which four input parameters other than normalization (N) are supplied (as mass of the BH is kept frozen at $14\,M_{\odot}$): (i) Keplerian disk rate ($\dot{m}_d$ in $\dot{M}_{\rm Edd}$), (ii) sub-Keplerian halo rate ($\dot{m}_h$ in $\dot{M}_{\rm Edd}$), (iii) location of the shock front (X_s in Schwarzschild radius $r_s = 2GM/c^2$) and (iv) compression ratio R(=ρ_+/ρ_-, i.e. ratio of post-shock to pre-shock density). In the TCAF model, two auxiliary parameters, namely, the mass of the BH (in solar mass $M_{\odot}$) and normalization (N) (it properly scales the entire model spectra up or down to match the observed spectra) are generally found to be constant. N depends on the intrinsic source parameters: mass of the BH, distance and disk inclination angle. So, in general N does not vary for a particular source (when observed with the same satellite instrument). But, one may require higher N values to fit spectra if there are significant effects of a jet or other physical processes, whose effects are not included in the present model fits file. To obtain best model fits, a Gaussian emission line of peak energy at around 6.5 keV is used to take care of the iron line emission.

Although $\chi_{2,4}$ classes are radio quiet, $\chi_{1,3}$ classes are radio loud i.e., there is significant radiation from jets or outflows. In the later two classes, the TCAF model was not sufficient to fit spectra due to the presence of outflows which could be emitting non-thermal X-rays (see C99, Jana et al. 2017). Thus, to obtain the best fit in these two classes, we applied an additional cutoffpl model. The cutoffpl profile is given by the equation $A(E) = KE^{-\alpha}\exp(-E/\beta)$, where α is the power-law photon index, β is the exponential roll-off in keV and K is the normalization in the unit of photons keV^{-1} cm^{-2} s^{-1}. The strength of α and β parameters will indicate relative dominance of the outflow in χ_1 and χ_3 classes and could shed some light regarding the accretion flow dynamics around the BH. In order to separate out the contributions from the TCAF system and the outflow system, we allowed the normalization parameter N to vary. Variation of the peak flux would be dependent on the variation of the accretion rates, and therefore, any error in determining the accretion rates would be reflected in the error of normalization. Even observational data quality may cause its fluctuation. Keeping these in mind, we first determined the energy range up to which the spectra could be fitted using the TCAF solution alone. This allows us to determine the average normalization which was kept frozen to obtain spectral fits in the $2.5 - 25$ keV energy range. Our procedure enabled us to separate the outflow contribution in the spectra following the method of Jana et al. (2017).

4 RESULTS

4.1 Analysis of χ_2 and χ_4 Classes

A comparison of the spectral natures of χ_2 class (Obs. Id. 20402-01-16-00) and χ_4 class (Obs. Id. 10408-01-33-00) implies that the energy flux is higher in χ_4 across the entire range of the spectra (Fig. 2). Since the spectral features

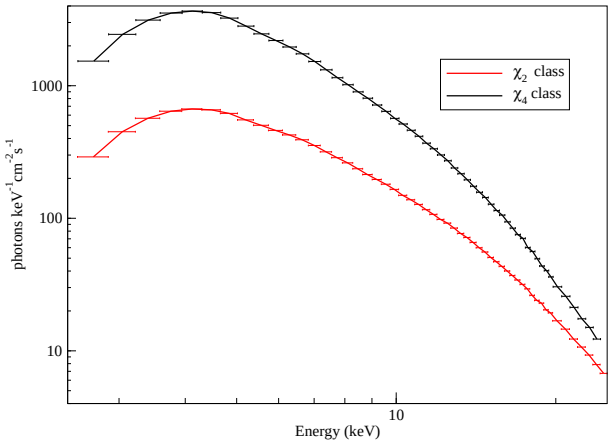

Fig. 2 Comparison of the observed spectra for χ_2 and χ_4 class data. The low energy flux in case of χ_4 class is greater than that of χ_2 class.

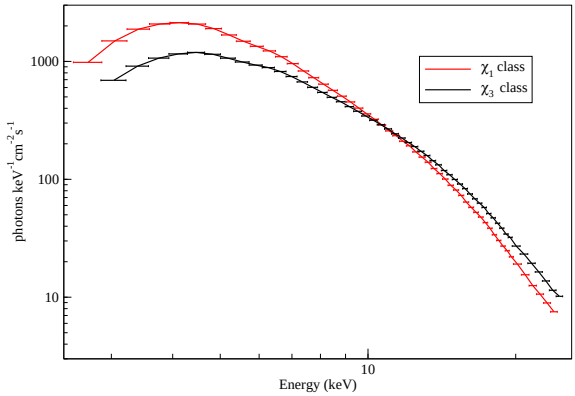

Fig. 3 Comparison of the spectra for χ_1 and χ_3 classes. The energy flux at lower energy is greater in case of the χ_1 class. The relative hardness of χ_3 class is apparent from the spectral slopes.

are ultimately governed by the accretion flow dynamics and consequently by the flow parameters, the different features of the observed spectra of $\chi_{2,4}$ classes should be corroborated by the spectral fitted parameters.

In the case of χ_2 class, a continuous observation spanning over 3000 seconds has been selected and fitted utilizing the TCAF+Gaussian model. The flow parameters, namely the disk accretion rate ($\dot{m}_d$), the halo rate ($\dot{m}_h$), shock location (X_s) and strength of the shock (R), have been determined. The same task has been done in case of χ_4 class data as well over the 800 second continuous observation span. The spectral fitted parameters for the two classes are mentioned in Table 1.

As is evident from the disk rate in case of the χ_4 class, the disk accretion rate is significantly larger compared to that of χ_2 class. This is in agreement with the higher low energy flux of χ_4 class data. However, since $\chi_{2,4}$ classes are devoid of any outflow, the normalization remains almost the same ($\sim$ 20). In case of the χ_4 class, the enhancement of disk rate makes the shock location move inwards. The data to model ratio for the fitted spectrum in χ_2 class is provided in Figure 5(a). In Figure 6(a), we produce the 66%–90%–99% contours for the fitted parameters $\dot{m}_d$ and $\dot{m}_h$ in the case of χ_2 class.

4.2 Analysis of χ_1 and χ_3 Class Data

We now summarize our findings from the spectral analysis of χ_1 and χ_3 class data. As mentioned earlier, unlike the $\chi_{2,4}$ class, substantial activity in the radio domain has been observed which implies the presence of an outflow. In order to account for the additional Comptonization from the base of the outflow, we applied the cutoffpl model in addition to the TCAF solution to fit the spectra in the $2.5-25$ keV energy range. A comparison of the nature of the observed spectra of χ_1 class (Obs Id. 10408–01–23–00) and χ_3 class (Obs Id. 20402–01–50–00) implies that the flux at lower energy is more in the case of the χ_1 class.

Because of the presence of an outflow, the spectral fitting solely with TCAF could not be accomplished over the entire range, but over only a restricted energy band. The relative hardness of χ_3 implies the difference in radio dominance in χ_1 and χ_3 classes. For this reason, the energy ranges of feasible TCAF fittings in these two classes were different.

Our objective was also to see whether contribution from TCAF and cutoffpl could be segregated. In that case, there would be a possibility that the accretion and outflow behaviors would be explainable independently without interference from one on another. For that purpose, after fitting the spectra using TCAF in the smaller energy range, the obtained normalization was kept frozen in the TCAF+cutoffpl fitting over the entire $2.5-25$ keV energy range.

• **Spectral fitting using *TCAF+cutoffpl* model for χ_1 class:** The continuous 3000 second observation was chosen for spectral fitting in the $2.5-25$ keV energy range. The disk rate and the TCAF normalization over the entire $2.5-25$ keV range were found to be around 1.75 $\dot{M}_{\rm Edd}$ and 17.5 respectively. The fitted spectral parameters employing the TCAF+cutoffpl model in the 2.5–25.0 keV have been listed in Table 2. The α and β parameters in the cutoffpl model have been found to be around 2.08 and 15.95 keV respectively. However, as stated earlier, because of the presence of outflow, the entire range could not be fitted with TCAF solely. In case of χ_1 class, only in the range 2.5-16.5 keV could the spectral fitting be accomplished applying TCAF only. The normalization was ascertained to be around 27.46.

Table 1 TCAF Model Fitted Parameters for χ_2 and χ_4 class data in the 2.5–25 keV energy band with the normalization as free. Variations of TCAF flow parameters, viz. disk accretion rate ($\dot{m}_d$), halo rate ($\dot{m}_h$), shock location (X_s), shock strength (R) and model normalization (N) with the chosen time segments along with the respective error bars, are listed. Reduced χ^2 of the spectral fits are expressed in the last column.

Variability class	$\dot{m}_d$ (in $\dot{M}_{\rm Edd}$)	$\dot{m}_h$ (in $\dot{M}_{\rm Edd}$)	X_s (in $M_\odot$)	R (in r_s)	N	χ^2/dof
χ_2	$0.797^{+0.02}_{-0.02}$	$0.161^{+0.001}_{-0.001}$	$47.302^{+0.07}_{-0.07}$	$1.233^{+0.001}_{-0.001}$	$22.125^{+0.016}_{-0.015}$	55.08/45
χ_4	$4.470^{+0.06}_{-0.06}$	$1.132^{+0.001}_{-0.001}$	$38.635^{+0.06}_{-0.06}$	$1.080^{+0.001}_{-0.001}$	$23.448^{+0.093}_{-0.092}$	46.84/44

Table 2 TCAF Model Fitted Parameters of χ_1 and χ_3 class PCA spectra in the 2.5–25 keV energy band with model normalization kept free. We have listed the variations of TCAF parameters, viz. disk accretion rate ($\dot{m}_d$), halo rate ($\dot{m}_h$), shock location (X_s), shock strength (R), model normalization (N) and cutoffpl parameters with the chosen time segments along with the respective error bars. The reduced χ^2 values of the spectral fits are also listed in the last column.

Variability class	$\dot{m}_d$ (in $\dot{M}_{\rm Edd}$)	$\dot{m}_h$ (in $\dot{M}_{\rm Edd}$)	X_s (in r_s)	R	N	α	β (in keV)	cutoffpl Norm	χ^2/dof
χ_1	$1.750^{+0.02}_{-0.02}$	$0.362^{+0.001}_{-0.001}$	$27.5^{+0.31}_{-0.27}$	$1.052^{+0.001}_{-0.001}$	$17.56^{+0.16}_{-0.16}$	$2.082^{+0.003}_{-0.002}$	$15.9^{+0.09}_{-0.09}$	$9.10^{+0.039}_{-0.038}$	35.92/41
χ_3	$1.131^{+0.01}_{-0.01}$	$0.182^{+0.003}_{-0.002}$	$20.1^{+0.03}_{-0.02}$	$1.438^{+0.002}_{-0.002}$	$2.85^{+0.06}_{-0.06}$	$1.563^{+0.01}_{-0.01}$	$15.7^{+0.08}_{-0.08}$	$3.23^{+0.003}_{-0.003}$	42.63/40

Table 3 TCAF Model Fitted Parameters for χ_1 and χ_3 class PCA spectra in the $2.5-25$ keV energy band with the normalization for TCAF frozen at the values as obtained from solely TCAF model fits over a smaller energy range. We have listed the variations of TCAF model parameters, viz. disk accretion rate ($\dot{m}_d$), halo rate ($\dot{m}_h$), shock location (X_s), the shock strength (R) and the additional cutoffpl model parameters with the chosen time segments along with the respective error bars. The reduced χ^2 values of the spectral fits are also listed in the last column.

Variability class	$\dot{m}_d$ (in $\dot{M}_{\rm Edd}$)	$\dot{m}_h$ (in $\dot{M}_{\rm Edd}$)	X_s (in r_s)	R	α	β (in keV)	cutoffpl Norm	χ^2/dof
χ_1	$2.494^{+0.04}_{-0.02}$	$0.367^{+0.002}_{-0.002}$	$32.434^{+0.11}_{-0.10}$	$1.052^{+0.006}_{-0.005}$	$1.871^{+0.04}_{-0.04}$	$13.674^{+0.02}_{-0.02}$	$6.323^{+0.04}_{-0.04}$	35.66/42
χ_3	$1.131^{+0.02}_{-0.01}$	$0.172^{+0.002}_{-0.002}$	$21.064^{+0.14}_{-0.14}$	$1.373^{+0.005}_{-0.004}$	$1.500^{+0.02}_{-0.02}$	$15.064^{+0.08}_{-0.08}$	$2.744^{+0.01}_{-0.01}$	40.48/41

The TCAF+cutoffpl fitting was repeated by keeping TCAF normalization frozen at $N = 27.46$ and the flow parameters were extracted. The parameters did not change significantly from those reported in Table 1. The fitted parameters are listed in Table 3. In Figure 5(b), the data to model ratio along with the individual components are depicted.

• **Spectral fitting using *TCAF+cutoffpl* model for χ_3 class:** We wanted to study the relative behavior of the χ_1 and χ_3 classes in terms of flow parameters. For that purpose, the same kind of spectral analysis as that of χ_1 class has been performed in the χ_3 class as well. In this case, a continuous 2000 second observation span had been chosen for spectral fitting utilizing the TCAF plus cutoffpl model in the $2.5-25$ keV range. The disk rate and the TCAF normalization over the entire $2.5-25$ keV range were obtained to be around 1.13 $\dot{M}_{\rm Edd}$ and 2.85 respectively. These are relatively lower than those of the χ_1 class, which were in agreement with the higher low energy flux in case of χ_1 class (Fig. 3). However, in case of χ_3 class since the sub-Keplerian accretion rate reduces compared to χ_1 class, the shock location moves inwards. Compared to the χ_1 class, the lower α and higher β in case of the χ_3 class were in conjunction with the relative hardness of χ_3 class data. The fitted parameters are listed in Table 2.

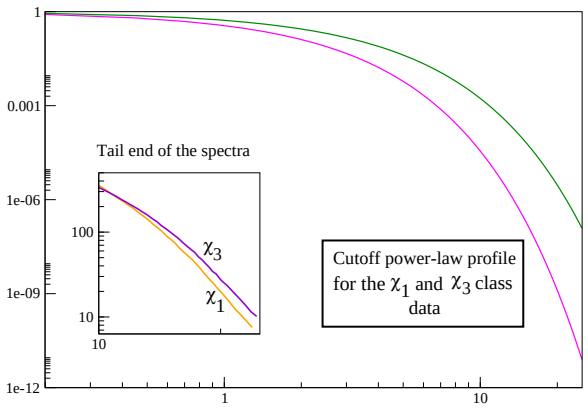

Fig. 4 Comparison of the cutoffpl profiles as obtained from the fitted parameters and tail end of the actual spectra. The relative hardness of χ_3 class as found from the fitted parameters is in agreement with the actual observation.

However, χ_3 class was harder, and the spectral fitting using only TCAF could be attained in the $2.5 - 14$ keV range. The disk rate obtained in this case was found to be lower as compared to the χ_1 class. The normalization was assessed to be around 5.55. The normalization for TCAF was frozen at this value and spectral fitting was repeated over the entire 2.5–25.0 band. The rest of the parameters were not ascertained to be changing significantly from those obtained from the parameters with normalization kept free. The cutoffpl parameters still conformed with the relative hardness of the χ_3 class. The lower disk rate for the χ_3 class accounting for smaller low energy flux was ensured in this case as well. The fitted parameters are listed in Table 3. In Figure 6(b), we provide the 1, 2 and 3σ contours of the parameters $\dot{m}_d$ and $\dot{m}_h$.

5 SUMMARY AND CONCLUDING REMARKS

Depending upon the nature of the variation in intensities, hardness, and other distinct spectral and timing properties, light curves of GRS 1915+105 were classified into 14 classes. IGR J17091–3624 is another BH, which belongs to this special category of objects and it also exhibits some of these class of light curves. The χ class has four different (χ_{1-4}) subclasses. In general, transient BHs show these characteristics of light curves in hard and hard-intermediate spectral states. These classes generally manifest steady variation of intensities or fluxes. However, we should mention one of the distinct differences in these four χ classes, such as jet or outflow nature. $\chi_{2,4}$ classes are radio-quiet whereas $\chi_{1,3}$ classes are radio-loud. In this paper, we concentrated on the χ class data and carried out spectral fits of all the four subclasses using the additive table model fits file, generated with the TCAF solution of Chakrabarti & Titarchuk (1995) after some necessary modifications (for more details, see Debnath et al. 2014, 2015b). We attempted to provide a plausible picture of the accretion flow dynamics. Given that in χ class observations of GRS 1915+105, the X-ray flux displayed negligible fluctuation and the spectra strikingly resemble the hard states of BHXBs, and given also that TCAF solution has been successful in explaining the spectral behavior of transient BHs in extracting physical flow parameters from fits, we were interested in looking at the spectral behavior of the χ class data of the variable source GRS 1915+105. This is the first time that such variable source data were fitted with the TCAF model. The theoretical backdrop for the explanation of the time variability of this kind of variable source under the purview of TCAF was envisaged by Chakrabarti and his collaborators (Fig. 1(a,b)). There it has been stated that the manifestation of all the different classes could be a consequence of the variation of the local accretion flow parameters, the emergence of outflow under suitable conditions, the collapse of outflow under sufficient cooling within the sonic radius ($\sim 2.5\ X_s$) and local enhancement of accretion flow because of return of a portion of the outflow (Chakrabarti et al. 2000). Among them, those flow configurations in which the flow is steady and outflow is absent; or those which are endowed with a steady outflow would be associated with a steady flux. They are identified as the χ classes, which we considered for our analysis in this paper. In case of $\chi_{2,4}$ classes which are devoid of outflow, the spectral fittings are accomplished with TCAF+Gaussian model only. Here, an additional Gaussian was included to account for the iron emission line at ~ 6.5 keV. Throughout the analysis, we have not kept the mass of the BH as a free parameter. This is because of the fact that mass is an intrinsic property of the BH and not a flow parameter. Since we are interested in the variation of flow parameters across different subclasses, we decided to peg the mass at a known value. The mass has been kept frozen at $14\ M_\odot$ as estimated in Greiner et al. (2001). This falls within the ballpark of more recent estimations of $12.4^{+2.0}_{-1.8}\ M_\odot$ by Reid et al. (2014). We observe that flow parameters do not significantly alter even if we change the mass $\sim 15\%$ within the observational ballpark. Even if we fix the mass at $\sim 12.4\ M_\odot$, the accretion rates change only $\sim$ 0.5% – 0.8%. Therefore, it does not affect our conclusions.

The low energy flux (< 10 keV) was significantly greater in the case of the χ_4 class. The disk rate of the χ_4 class turned out to be more as compared to that of the χ_2 class since the disk photons primarily contribute to the lower energy end of the spectra. However, since the outflow is not present, the normalizations between these classes are almost the same (see Table 1).

If we compare the spectral nature of χ_2 and χ_4 classes, we observe a higher photon energy flux in both soft and hard domains in the case of the χ_4 class (Fig. 2). The ratio of energy flux in harder (10.0–25.0 keV) and softer (2.5–10.0 keV) domains turns out to be ~ 0.32 and 0.63 in cases of the χ_2 and χ_4 classes respectively. Therefore, the flux of high energy photons appears to be more in the case of the χ_2 class. However, the ratio of halo accretion rate and disk accretion rate in the case of χ_2 and χ_4 turns out to be 0.20 and 0.25 respectively. This apparent paradox is resolved when one notes that the flux does not depend only on the accretion rates, but on all the flow parameters, such as the shock location and shock strength. For this reason, the ratio of fluxes between two classes cannot be equated with just the accretion rate ratios. If we had a controlled system where one accretion rate can be changed keeping other parameters constant then such comparisons would make sense. In our case, the shock location decreases from $\sim 47\ r_s$ to $\sim 38\ r_s$ as we move from χ_2 to χ_4 class. Shock strength also does not remain constant. Higher shock location and stronger shock in case of the χ_2 class

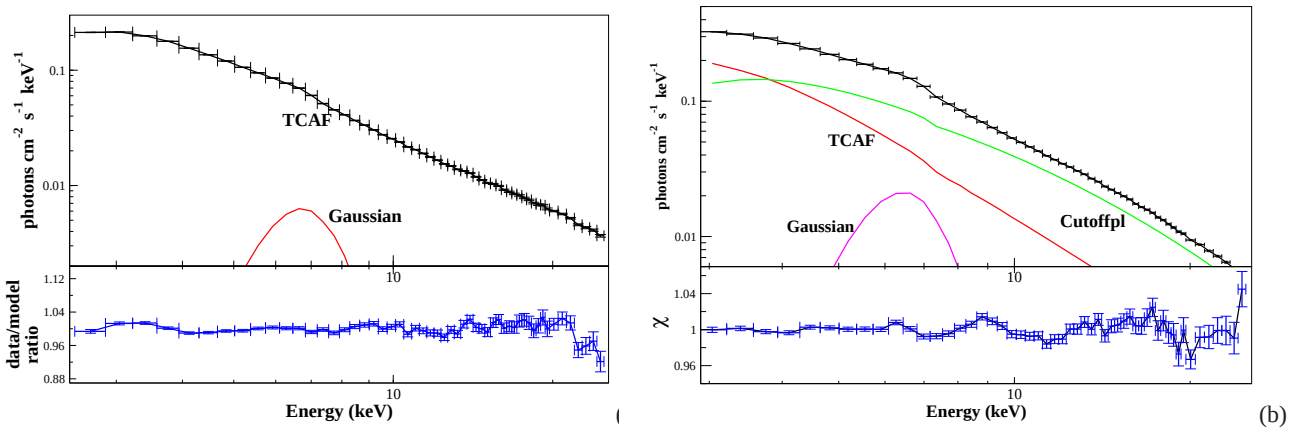

(a) (b)

Fig. 5 (a) The data to model ratio for a fit in the χ_2 class data using the *TCAF* model. A Gaussian is added to take into account the iron line emission ~ 6.5 keV. (b) The data to model ratio for fitted spectrum of χ_1 class data applying *TCAF + cutoffpl* model. The Gaussian profile for iron Kα line emission is added.

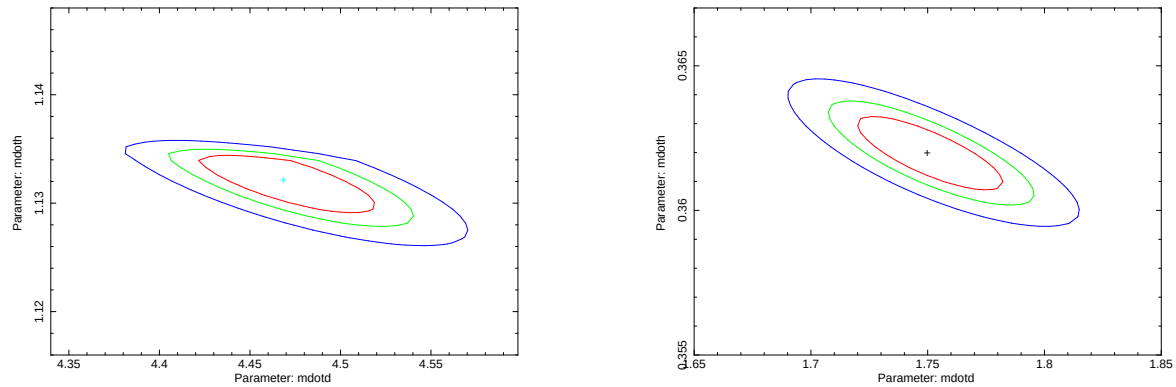

Fig. 6 The $66\% - 90\% - 99\%$ confidence contours for the fitted parameters $\dot{m}_d$ and $\dot{m}_h$ in the case of χ_4 and χ_1 classes respectively are presented in (a) and (b).

naturally intercepts more soft photons and consequently produces more hard photons through inverse Compton scattering. All such factors contribute to the overall flux and hardness of the spectra. However, if we compute the contribution of TCAF in the overall energy flux in 2.5–25.0 keV, we observe that in the case of the χ_4 class the flux is greater by a factor of ~ 4.8 compared to the χ_2 class. This result is in agreement with Figure 2.

The launching of outflow from within the CENBOL region would be sensitive to the flow parameters. It was shown in C99 that outflows from CENBOL are possible in harder states. The process is not sensitive to the total accretion rate, but rather the location of the shock and the compression ratio R at the CENBOL boundary. Often high accretion rates quench the jet base and reduce the thermal pressure required for the launching of jets. In the case of the $\chi_{1,3}$ class, the outflow is collimated and steady. Consequently, the inverse Comptonization of seed photons from the base of the outflow is present and that is manifested as an additional power-law. We had to employ the cutoffpl model in addition to TCAF for best spectral fitting. The two parameters α (the power-law photon index) and β (the exponential roll-off factor) dictate the strength of the outflow. From the comparison of the spectral nature of the two classes, the relative dominance of low energy flux for the χ_1 class data and also its overall relative hardness are apparent. These two features must be reflected in the spectral fitted parameters. In the $\chi_{1,3}$ class data, since the cooling within the sonic sphere is not catastrophic and there is no fall back of the outflow on the initial accreting matter, the fitted parameters also must not change over the period of observation. These are the features that were actually obtained as has been reported earlier. The disk rate as obtained in the case of χ_1 class data was dominant over χ_3 class. The lower α and higher β of χ_3 class data accounted for the relative hardness of that class. The work done by Rao et al. (2000) resolved the χ_3 class data into multi-color disk blackbody,

a Comptonized component and a power-law by fitting the spectra with diskbb+CompST+cutoffpl model. Since the disk and Comptonized component from the CENBOL have been already incorporated in the TCAF solution, only the addition of cutoffpl model along with the TCAF solution should be sufficient to account for the contribution from the outflow. The result we have obtained thus vindicated our expectation. However, in order to segregate the contributions from the two components, we did the spectral fitting in two phases. Using TCAF solely, the spectra were fitted in a smaller energy range. Subsequently, the spectral analysis was repeated in the entire $2.5 - 25.0$ keV energy range with the TCAF+cutoffpl model keeping the TCAF normalization frozen at the average value from the earlier fitting. The values of the fitted parameters did not change significantly, and the essential relative features between the spectra of χ_1 and χ_3 class data still remained. Thus the one-to-one correspondence of the $\chi_{1,3}$ class of the object with the accretion flow configuration as depicted in Figure 1(a,b) is justified, with the effect of Comptonization being absorbed in the cutoffpl model. The relative dominance of outflow in the case of χ_3 class data is corroborated well from the α and β parameters.

From Figure 5(b), we observe that the cutoffpl contribution starts dominating over TCAF above $\sim$ 4 keV. However, this still does not make TCAF redundant. Cutoffpl is added to account for the power-law contributed by inverse Comptonized photons from the outflow base. The outflow, on the other hand, is launched from within the CENBOL region, which, in turn, is produced because of the interplay of accretion rates. Therefore, the accretion flow and outflow together form a complete system. Therefore, the description of the system can be complete only if both of these segments are described by respective models. The cutoffpl parameters are indicative of the relative strength of the outflow in different subclasses, which is depicted in Figure 4.

Earlier, all the classes of this interesting source GRS 1915+105 were characterized by the CE, which is nothing but the ratio of power-law and blackbody photons (Pal et al. 2011). This is different from the standard hardness ratio because the energy domain corresponding to soft and hard photons dynamically varies from one class to another. This is a measure of geometrical variation and how the CENBOL is evolving as the source transits from one class to another. Therefore, the sequencing of CE in ascending order provides us a plausible sequence of transition of the source from one variability class to another. On the other hand, spectral fitting of the observed spectra using TCAF provides us a description of the accretion flow around the source in different classes in terms of basic flow parameters. In case of TCAF, the soft and hard fluxes are not calculated separately. Rather, all the flow parameters contribute to fit the observed spectral energy distribution. For this reason, the individual flow parameters or their ratios cannot be connected to the CE of respective classes. Rather, all the flow parameters are important for a meaningful description of each individual subclass. Also, incorporation of associated phenomenological models like cutoffpl can provide us information regarding strength of the outflow present in different subclasses. Therefore, spectral fit utilizing physical models of TCAF provides us a deeper understanding of the characteristics of different subclasses in terms of accretion flow dynamics. In Banerjee et al. (2020), TCAF has already been applied to study the flow parameters in case of θ class data of GRS 1915+105.

The next logical step would be to embark upon the spectral analysis on intermediate classes that present a wide range of time variabilities. We believe that the root of such variabilities is the changing configurations of the accretion flow and during the transition from burst-off to burst-on state the accretion rates and the normalization would change accordingly to suit that feature. This process is underway and the results will be reported elsewhere.

Acknowledgements A.B. and A.B. acknowledge support from a fellowship of the S. N. Bose National Centre for Basic Sciences, Kolkata, India. D.D. acknowledges partial support from the DST/GITA sponsored India-Taiwan (China) collaborative project fund (GITA/DST/TWN/P-76/2017). S.K.C. and D.D. acknowledge partial support from the ISRO sponsored RESPOND project (ISRO/RES/2/418/17-18) fund. Research of D.D. and S.K.C. is supported in part by the Higher Education Dept. of the Govt. of West Bengal, India. We would also like to thank the anonymous referee, whose comments and suggestions have contributed to enhance the quality of this paper.

References

Banerjee, I., Bhattacharjee, A., Banerjee, A., Debnath, D., & Chakrabarti, S. K. 2019, arXiv:1904.11644

Banerjee, A., Bhattacharjee, A., Chatterjee, D., et al. 2020, arXiv:2007.05273

Belloni, T., Klein-Wolt, M., Méndez, M., van der Klis, M., & van Paradijs, J. 2000, A&A, 355, 271

Bhattacharjee, A. 2018, in Exploring the Universe: From Near Space to Extra-Galactic, eds. B. Mukhopadhyay, & S. Sasmal, 53, 93

Bhattacharjee, A., Banerjee, I., Banerjee, A., Debnath, D., & Chakrabarti, S. K. 2017, MNRAS, 466, 1372

Bhattacharjee, A., & Chakrabarti, S. K. 2017, MNRAS, 472, 1361

Bhattacharjee, A., & Chakrabarti, S. K. 2019, ApJ, 873, 119

Blum, J. L., Miller, J. M., Fabian, A. C., et al. 2009, ApJ, 706, 60

Chakrabarti, S. K. 1995, in Seventeeth Texas Symposium on Relativistic Astrophysics and Cosmology, eds. H. Böhringer, G. E. Morfill, & J. E. Trümper, 759, 546
Chakrabarti, S., & Titarchuk, L. G. 1995, ApJ, 455, 623
Chakrabarti, S. K. 1997, ApJ, 484, 313
Chakrabarti, S. K. 1999, A&A, 351, 185 (C99)
Chakrabarti, S. K., & Manickam, S. G. 2000, ApJL, 531, L41
Chakrabarti, S. K., Manickam, S. G., Nandi, A., & Rao, A. R. 2000, astro-ph/0012525
Chakrabarti, S. K., & Nandi, A. 2000, arXiv e-prints, astro-ph/0012526
Chatterjee, D., Debnath, D., Chakrabarti, S. K., Mondal, S., & Jana, A. 2016, ApJ, 827, 88
Chatterjee, D., Debnath, D., Jana, A., & Chakrabarti, S. K. 2019, Ap&SS, 364, 14
Chatterjee, K., Debnath, D., Chatterjee, D., Jana, A., & Chakrabarti, S. K. 2020, MNRAS, 493, 2452
Debnath, D., Chakrabarti, S. K., & Nandi, A. 2013, AdSpR, 52, 2143
Debnath, D., Chakrabarti, S. K., & Mondal, S. 2014, MNRAS, 440, L121
Debnath, D., Molla, A. A., Chakrabarti, S. K., & Mondal, S. 2015a, ApJ, 803, 59
Debnath, D., Mondal, S., & Chakrabarti, S. K. 2015b, MNRAS, 447, 1984
Debnath, D., Jana, A., Chakrabarti, S. K., Chatterjee, D., & Mondal, S. 2017, ApJ, 850, 92
Debnath, D. 2018, in Exploring the Universe: From Near Space to Extra-Galactic, eds. B. Mukhopadhyay & S. Sasmal, 53, 229
Debnath, D., Chatterjee, D., Jana, A., Chakrabarti, S. K., & Chatterjee, K. 2020, RAA (Research in Astronomy and Astrophysics), 20, 175
Fender, R., & Belloni, T. 2004, ARA&A, 42, 317
Fender, R. P., Belloni, T. M., & Gallo, E. 2004, MNRAS, 355, 1105
Garain, S. K., Ghosh, H., & Chakrabarti, S. K. 2012, ApJ, 758, 114
Ghosh, A., & Chakrabarti, S. K. 2019, MNRAS, 485, 4045
Giri, K., & Chakrabarti, S. K. 2013, MNRAS, 430, 2836
Greiner, J., Morgan, E. H., & Remillard, R. A. 1996, ApJL, 473, L107
Greiner, J., Cuby, J. G., McCaughrean, M. J., Castro-Tirado, A. J., & Mennickent, R. E. 2001, A&A, 373, L37
Jana, A., Debnath, D., Chakrabarti, S. K., Mondal, S., & Molla, A. A. 2016, ApJ, 819, 107
Jana, A., Chakrabarti, S. K., & Debnath, D. 2017, ApJ, 850, 91
Jana, A., Debnath, D., Chakrabarti, S. K., & Chatterjee, D. 2020a, RAA (Research in Astronomy and Astrophysics), 20, 028
Jana, A., Debnath, D., Chatterjee, D., et al. 2020b, ApJ, 897, 3
Klein-Wolt, M., Fender, R. P., Pooley, G. G., et al. 2002, MNRAS, 331, 745
Lee, J. C., Reynolds, C. S., Remillard, R., et al. 2002, ApJ, 567, 1102
McClintock, J. E., & Remillard, R. A. 2006, Black Hole Binaries, 39, Compact Stellar X-ray Sources, 39 (Cambridge, UK: Cambridge University Press), 157
Molla, A. A., Debnath, D., Chakrabarti, S. K., Mondal, S., & Jana, A. 2016, MNRAS, 460, 3163
Mondal, S., Debnath, D., & Chakrabarti, S. K. 2014, ApJ, 786, 4
Mondal, S., Chakrabarti, S. K., & Debnath, D. 2016, Ap&SS, 361, 309
Morgan, E. H., Remillard, R. A., & Greiner, J. 1997, ApJ, 482, 993
Muno, M. P., Morgan, E. H., & Remillard, R. A. 1999, ApJ, 527, 321
Naik, S., & Rao, A. R. 2000, A&A, 362, 691
Pal, P. S., Chakrabarti, S. K., & Nandi, A. 2011, IJMPD, 20, 2281
Pal, P. S., Chakrabarti, S. K., & Nandi, A. 2013, Advances in Space Research, 52, 740
Pal, P. S., & Chakrabarti, S. K. 2015, Advances in Space Research, 56, 1784
Peris, C. S., Remillard, R. A., Steiner, J. F., et al. 2016, ApJ, 822, 60
Rao, A. R., Naik, S., Vadawale, S. V., & Chakrabarti, S. K. 2000, A&A, 360, L25
Reid, M. J., McClintock, J. E., Steiner, J. F., et al. 2014, ApJ, 796, 2
Remillard, R. A., & McClintock, J. E. 2006, ARA&A, 44, 49
Shang, J. R., Debnath, D., Chatterjee, D., et al. 2019, ApJ, 875, 4
Smith, D. M., Heindl, W. A., & Swank, J. H. 2002, ApJ, 569, 362
Sunyaev, R. A., & Titarchuk, L. G. 1980, A&A, 500, 167
Sunyaev, R. A., & Titarchuk, L. G. 1985, A&A, 143, 374
Vadawale, S. V., Rao, A. R., Nandi, A., & Chakrabarti, S. K. 2001, A&A, 370, L17
Vadawale, S. V., Rao, A. R., Naik, S., et al. 2003, ApJ, 597, 1023
Wu, K., Soria, R., Campbell-Wilson, D., et al. 2002, ApJ, 565, 1161
Yadav, J. S., Rao, A. R., Agrawal, P. C., et al. 1999, ApJ, 517, 935
Yadav, J. S. 2001, ApJ, 548, 876
Yadav, J. S. 2006, ApJ, 646, 385